



Contents lists available at ScienceDirect

## Chemical Engineering Journal

journal homepage: [www.elsevier.com/locate/cej](http://www.elsevier.com/locate/cej)Thermodynamic modeling for the carbonate system K-HCO<sub>3</sub>-CO<sub>3</sub> in alkanolamine solutions: An extended application for CO<sub>2</sub> scrubbingQiaoxin Wang<sup>a,b</sup>, Zhibao Li<sup>a,\*</sup><sup>a</sup> Key Laboratory of Green Process and Engineering, Institute of Process Engineering, Chinese Academy of Sciences, Beijing 100190, China<sup>b</sup> Dept. of Chemical Engineering, University of Chinese Academy of Sciences, Beijing 100049, China

## HIGHLIGHTS

- The construction of a thermodyn. framework for the system: K<sub>2</sub>CO<sub>3</sub>-MEA/DEA-CO<sub>2</sub>-H<sub>2</sub>O.
- A chemical model was built after solubility tests and through data regression.
- The amine composition and temperature directly affect the solubility of K<sub>2</sub>CO<sub>3</sub> and KHCO<sub>3</sub>.
- Carbamate increases until  $\alpha$  reaches 0.45 for K-CO<sub>3</sub><sup>2-</sup>-amine solutions at 313 K.
- No complex ion is formed if K<sup>+</sup> is added, it only increases the mass transfer rate.

## ARTICLE INFO

## Keywords:

Alkanolamine  
Solid-liquid equilibrium  
Modeling  
Solubility  
Thermodynamics

## ABSTRACT

The K<sub>2</sub>CO<sub>3</sub> slurry-based, CO<sub>2</sub> absorption technology in amines involves in-depth analysis of chemical equilibrium for all three phases. However, the reported studies regarding solubility and thermodynamics modeling of the solid-liquid system: K-CO<sub>3</sub>-HCO<sub>3</sub> in alkanolamine solutions are limited. We first performed vapor-liquid equilibrium calculation to study the absorption profile of CO<sub>2</sub> in monoethanolamine (MEA) /diethanolamine (DEA) solutions using OLI Studio Stream Analyzer, results were in good agreement with literature data. We further applied the dissolution method to measure the solubility of K<sub>2</sub>CO<sub>3</sub> and KHCO<sub>3</sub> in the aqueous alkanolamine solution from 283 to 353 K,  $P = 0.1$  MPa. A chemical model was developed for the purpose of conducting thermodynamic analysis by the regression of solubility data via the mixed-solvent-electrolyte, activity coefficient model. The relative deviations are within 5% for each solid-liquid system after reparameterization. Tuning the newly-regressed parameters allowed for a better prediction of solubility, they also come vital in evaluating the absorption performance of CO<sub>2</sub> in quaternary systems, which are made available to aid in process modeling.

## 1. Introduction

The post-combustion capturing (PCC) technique is one of the most mature technology to reduce carbon emission at present, and it is anticipated to be a sustainable technology in the future for greater-in-scale commercialization [1–3]. For example, PCC technique has been used to remove acidic gas such as CO<sub>2</sub> and H<sub>2</sub>S in conventional LNG plants [4,5]. Over the past decades, scientists and researchers are dedicated to

optimize the CO<sub>2</sub> absorption process, many have found that amine additives such as monoethanolamine (MEA), diethanolamine, (DEA) as well as other ionic liquids are capable of improving the absorption efficiency [6–9]. Among those, DEA is a secondary amine, it shows advantages in the treatment of acidic gas due to a higher capacity, lower cost, and a limited formation of carbamate [10]. Results were often interpreted in the term of shuttle mechanism [11]. Furthermore, the presence of acidic gas tends to result in equipment corrosion and

**Abbreviations:** MSE, Mixed-Solvent-Electrolyte; wt%, weight percentage;  $a_{0,ij}$ ,  $a_{1,ij}$ ,  $a_{2,ij}$ ,  $a_{0,ji}$ ,  $a_{1,ji}$ , and  $a_{2,ji}$ , MSE, Model: short-range adjustable parameters;  $b_{0,ij}$ ,  $b_{1,ij}$ ,  $b_{2,ij}$ , and  $b_{3,ij}$ , MSE Model, middle-range adjustable parameters;  $k_{ij0}$ ,  $k_{ij1}$ ,  $k_{ij2}$ , MSE Model: parameters for fugacity coefficients;  $Q_{iij}$ ,  $Q_{iJI}$  ( $i = 1, 2, \dots$ ), short-range adjustable parameters of the MSE Model;  $g_{ij}$ , MSE Model: Kabadi-Danner extension parameter;  $B_{ij}$ , middle-range interaction parameter between species  $i$  and  $j$ ;  $c_{ij}$ , middle-range interaction parameter between species  $i$  and  $j$ ;  $I_{\pm}$ , mole-fraction-based ionic strength;  $m$ , molality (mol/kg solvent);  $R$ , ideal gas constant ( $8.314 \text{ J mol}^{-1} \text{ K}^{-1}$ );  $x_i$ , mole fraction of species  $i$ ;  $\gamma_i$ , activity coefficient of species  $i$ ;  $\mu_i^{G,0}(T)$ , chemical potential of pure component  $i$ ;  $\varphi_i(T,P)$ , fugacity coefficient; SRK EoS, Soave-Redlich-Kwong (SRK) cubic equation of state (EoS); VLSE, Vapor-Liquid-Solid-Equilibrium

\* Corresponding author.

E-mail address: [zhibao.li@ipe.ac.cn](mailto:zhibao.li@ipe.ac.cn) (Z. Li).<https://doi.org/10.1016/j.cej.2019.123250>

Received 4 August 2019; Received in revised form 29 September 2019; Accepted 19 October 2019

1385-8947/© 2019 Elsevier B.V. All rights reserved.

pipeline clogging, so the gas sweetening process must be in focus to prevent equipment failure [12].

It is well-known that potassium carbonate ( $K_2CO_3$ ), aka. hot potash solutions, are among the most prevalent solvent particularly effective to improve the overall performance of  $CO_2$  absorption [12–14]. Here the biggest challenge is the low in the rate of reaction, resulting in poor  $CO_2$  mass transfer if carbonate solution is used alone [14]. By the addition of amine promoters such as MEA or DEA, the rate of absorption can be greatly enhanced.  $K_2CO_3$  is thermally stable due to its physical nature even if temperature exceeds 373 K. Compared to other sorbents such as  $K_2SO_4$  and  $Na_2SO_4$ ,  $K_2CO_3$  outperforms in terms of reaction rate. Specifically, Laddha et al. [15] reported that in a solution containing 1 mol/L of DEA, the rate of absorption accelerates for a factor of 2.1 if the concentration of  $K_2CO_3$  increases from 0 to 1 mol/L ( $T = 298$  K). Under the same condition, the rate of absorption decreases for a factor of 0.8 if  $Na_2SO_4$  is used instead. Moreover, recent researches conducted from the perspective of life cycle analysis [13] concludes that the absorption of acidic gas using carbonate solvents, or  $NH_3$  solution in alternative, tends to have lower environmental impact compared to other inorganic solvents. Therefore, with the potential of achieving large-scale  $CO_2$  mitigation in power plant, selecting the system containing  $K_2CO_3-HCO_3$  in both MEA and DEA solutions would be very beneficial for process design and optimization.

An integrated, gas scrubbing process (aka. HiPure Process) is presented in Fig. 1 [16,17]. It uses the potassium carbonate solution, promoted with DEA to remove  $CO_2$  by integrating two, independent circulations. This process has been used industrially to treat  $CO_2$  of < 50 ppmv, and is able to remove  $CO_2$  while meeting the 20 ppmv specification. First, the carbonate solution (~30 wt%  $K_2CO_3$ , 3 wt% DEA) absorption column takes in the feed gas, then transfers it into the amine absorption column containing 20 wt% DEA. After the second absorption process reaches completion, the rich amine solution from the absorber is loaded into the amine regenerator. The overhead gas is then transported into the carbonate regenerator. The liquid from the carbonate regenerator condenser, (up-right corner) is fed into the amine regenerator as reflux. The sweetened gas being treated after this stage will undergo further processes to meet the desired purity [16,17].

However, conditions when solids may form during the absorption process remains unknown if a higher concentration of amine solution is needed to treat acidic gas, further promoted by  $K_2CO_3$  to increase the rate of absorption. As such, finding the maximum solubility of  $K_2CO_3$  which can be dissolved into amine solutions is significant. Altogether, the objective of this study is to develop a comprehensive thermodynamic model to describe the properties of the solvent system including vapor-liquid equilibrium, solid-liquid equilibrium, and combined vapor-liquid-solid equilibrium. To advance the state of knowledge and technology regarding  $CO_2$  absorption, this model can be further utilized to predict the formation of solid under different experimental condition. Speciation profile of electrolytes are constructed to visualize the change in dominant species. Given that  $CO_2$  reacts rapidly with amine, the model brings conveniences for the estimation of  $CO_2$  partial pressure, avoiding the complexity of using  $N_2O$  analogy experimentally [11]. We consider a model reliable for the direct calculation of  $CO_2$  solubility up to the maximum carbonate/amine loading capacity only if both vapor-liquid, and solid-liquid interaction parameters are accurate. For both systems: MEA- $CO_2$ - $H_2O$  and DEA- $CO_2$ - $H_2O$ , we graphically illustrated our computed results with respect to  $P_{CO_2}$ , and had plotted the results taken from literature works. Most importantly, this work reports the solubility data for the four, proposed solid-liquid systems:  $K_2CO_3$ -MEA- $H_2O$ ,  $KHCO_3$ -MEA- $H_2O$ ,  $K_2CO_3$ -DEA- $H_2O$ ,  $KHCO_3$ -DEA- $H_2O$  between 283 and 353 K,  $P = 0.1$  MPa. Regression/correlation of data were achieved by adjusting the ion-ion interaction parameters using OLI Analyzer 9.6, calculated using the mixed-solvent electrolyte (MSE) model [18].

## 2. Experimental

### 2.1. Materials

Chemical substances such as potassium carbonate ( $K_2CO_3$ ) and potassium bicarbonate ( $KHCO_3$ ) were used for experimental purposes. Both chemicals were obtained in the form of solid. In addition, monoethanolamine (MEA) and diethanolamine (DEA) were supplied by Xilong Scientific. Deionized water with a specific conductivity of

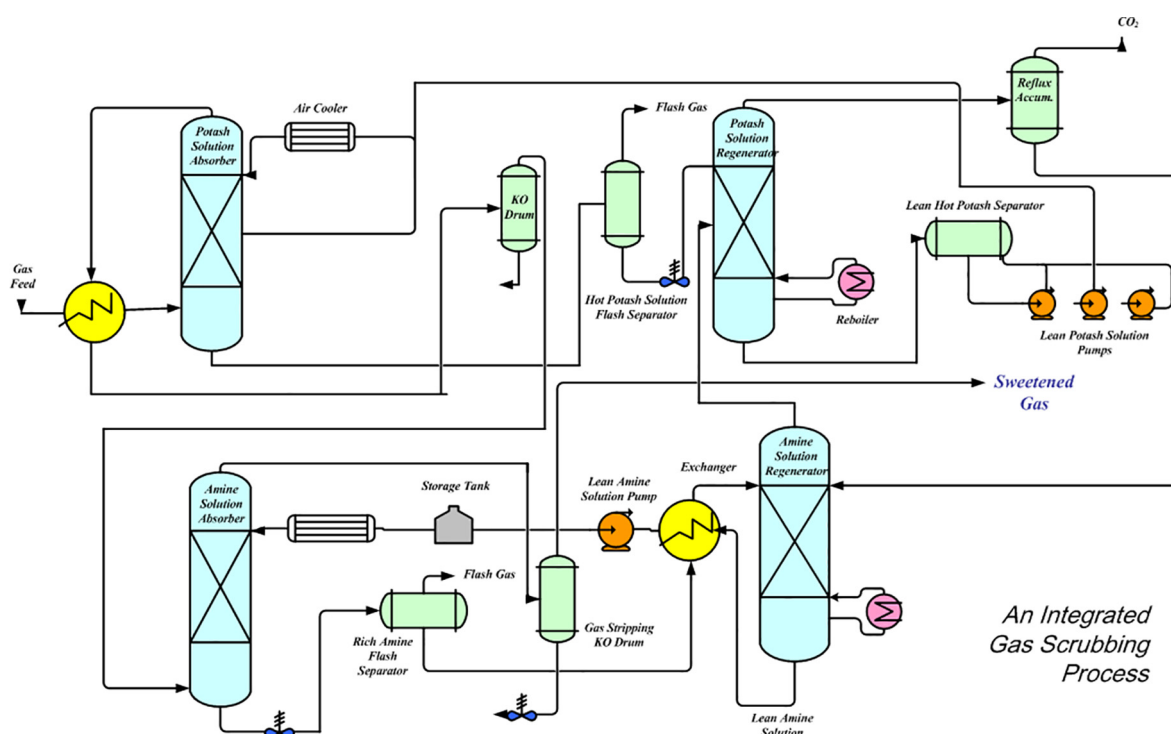

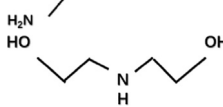
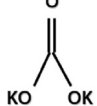
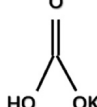


Fig. 1. An integrated gas scrubbing process.

**Table 1**  
A List of Chemical Reagents.

Chemical Compound	Structure	Supplier	Analytical Purity
Monoethanolamine (MEA)		XiLong Scientific	≥0.995
Diethanolamine (DEA)		XiLong Scientific	≥0.995
Potassium Carbonate (K <sub>2</sub> CO <sub>3</sub> )		SinoPharm	≥0.99
Potassium Bicarbonate (KHCO <sub>3</sub> )		SinoPharm	≥0.995

0.1 μS cm<sup>-1</sup> was used throughout this experiment. Details for chemical specifications are collectively shown in Table 1.

## 2.2. Procedure

Prior to conducting the solid-liquid solubility experiments, we first computed the partial pressure of CO<sub>2</sub> vs. loading capacity α (mol CO<sub>2</sub>/mol amine) for the system: MEA-H<sub>2</sub>O-CO<sub>2</sub> and DEA-H<sub>2</sub>O-CO<sub>2</sub> using the existing vapor-liquid interaction parameters. These simulated results were evaluated using the reported literature data. Afterwards, the solubility measurements for the proposed, solid-liquid systems: K<sub>2</sub>CO<sub>3</sub>-MEA-H<sub>2</sub>O, KHCO<sub>3</sub>-MEA-H<sub>2</sub>O, K<sub>2</sub>CO<sub>3</sub>-DEA-H<sub>2</sub>O and KHCO<sub>3</sub>-DEA-H<sub>2</sub>O were carried out in this order. As for measurements, the amount of amine, water, and solutes (K<sub>2</sub>CO<sub>3</sub> and KHCO<sub>3</sub>) were weighed out on a mass balance (Mettler Toledo, model AL104) in the unit of grams. Grams are further converted into molal scale: mol/kg<sub>H2O</sub> for the easiness of parameterization. Solubilities for the systems proposed were determined via the ‘dissolution method’. The two independent variables set to change were temperature: 283–353 K; and the concentration of amine: 0–10 mol/kg. During the experiment, we used a mass balance with the precision of 0.001, and a thermostat (Scientz, DC-1015) to control the temperature. Multiple sets of magnetic stirring plates (Shanghai Sile Co., 84-1A) were turned on and placed under the jacketed-reactors to initiate continuous stirring motions. All solubility experiments were conducted at atmospheric pressure.

After taken the solubility measurements for the proposed solid-liquid systems, we compiled these data and had successfully regressed the relevant, unitless parameters by incorporating pairwise-ion interactions [18,19]. The OLI Analyzer 9.6 – a software developed by OLI Systems Inc. [20–22] was used as a computational tool to predict the solubility of salts at first, parameters were later modified using the

Brown algorithm embedded in the OLI Engine Solver; this was essentially the most critical step prior to constructing a comprehensive thermodynamic model. At last, the model was built by incorporating the newly-regressed parameters. The experimental solubility data, together with the predicted solubility of CO<sub>2</sub> in the quaternary systems were further plotted. Detailed analysis for the results obtained are discussed in the subsequent sections.

## 3. Thermodynamic frameworks

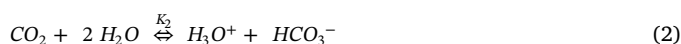
### 3.1. Solution chemistry

Like other amines, MEA or DEA acts as a weak base [11,13]. The intermediate formation of the carbamate is only a single-step reaction – a loosely bounded, small fraction of ionic product. General dissociation equations are shown in Eqs. (1)–(5), and the equilibrium constants associated with each equation are listed in Table 2. Herein R<sub>2</sub>NH is the alkanolamine, R<sub>2</sub>NCOO<sup>-</sup> is the formed, carbamate intermediate [10,23–25].

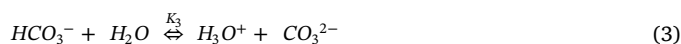
#### 1. Water ionization



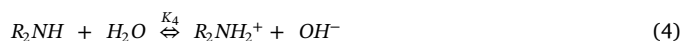
#### 2. Dissociation and hydrolysis of CO<sub>2</sub>



#### 3. Dissociation of bicarbonate ion



#### 4. Dissociation of the protonated amine



#### 5. Carbamate species reversion to bicarbonate ion



These reactions are considered to be reversible. Any additional reactions than the ones shown may produce non-regenerable heterocyclic compound, we chose not to include these reactions as they are insignificant during the gas sweetening simulation process.

### 3.2. VLE thermodynamic framework: SRK

Constructing a comprehensive thermodynamic model capable of calculating the partial pressure of CO<sub>2</sub> regarding the VLE systems: MEA-H<sub>2</sub>O-CO<sub>2</sub>, DEA-H<sub>2</sub>O-CO<sub>2</sub> is essential for gas sweetening process simulations. To our knowledge, literature works unveiled that considerable progress has been made in modeling the VLE data in determining both physical and chemical properties for these systems. OLI Stream Studio Analyzer was utilized for computational purposes. In addition, the

**Table 2**  
A List of Equilibrium Constants for All Dissociation Equations.

$k_{1-5}$	Expression/Parameters	Ref.
$k_1$	$\log(k_1) = -5839.5/T - 22.4773 \log(T) + 61.2062$	OLI PUB
$k_2$	$\log(k_2) = 14.19574 - 3312.21517/T - 0.0433 T - 0.000019319 T^2$	Ref. [26]
$k_3$	$\log(k_3) = 10.55112 - 3528.2283/T - 0.04177 T - 0.00001861 T^2$	Ref. [26]
$k_{4, \text{MEA}}$	$\log(k_{4, \text{MEA}}) = 12.4361 - 2257.2/T - 0.04115 T + 0.000032318 T^2$	OLI PUB
$k_{4, \text{DEA}}$	$\log(k_{4, \text{DEA}}) = 15.7444 - 2951.4/T - 0.04886 T + 0.00004056 T^2$	OLI PUB
$k_{5, \text{MEACOO-}}$	$\log(k_{5, \text{MEACOO-}}) = 80.3786 - 8433.6/T - 0.259151 T + 0.000275487 T^2$	OLI PUB
$k_{5, \text{DEACOO-}}$	$\log(k_{5, \text{DEACOO-}}) = 9.49186 - 3091.66/T - 0.009582 T + 0.000030166 T^2$	OLI PUB

\* $k_2$  and  $k_3$  are refitted using eq.  $\log(k) = A + B/T + CT + DT^2$  [21].

usage of the MSE model is further extended by incorporating the adjusted parameters to visualize how the presence of solids, from a low concentration to the maximum loading possible, would influence the solubility of CO<sub>2</sub> through the calculation of  $P_{CO_2}$  under various amine compositions and temperature.

First, the aqueous electrolyte dissociates into the liquid phase can be represented by the combination of both the Helgeson–Kirkham–Flowers (HKF) equation of state for ground state properties [27], as well as the activity coefficient model which accounts for a non-ideal solution [28]. The HKF model accounts for thermodynamic properties of species, and the equilibrium constants for reactions up to 1000 °C and 5 kbar. Eq. (6) only taken into account of the liquid phase, which contains both water and amine in our case. Note that the liquid phase is also the phase that contains the dissolved, aqueous electrolytes.

$$\mu_i^L = \mu_i^{L,0,x}(T, P) + RT \ln x_i \gamma_i X(T, P, x) \quad (6)$$

In this equation,  $\mu_i^{L,0,x}(T, P)$  is the chemical potential derived from HKF,  $x_i$  is the mole fraction, and  $\gamma_i X(T, P, x)$  is the activity coefficient; it accounts for long-range electrostatic, middle-range interactions, and short-range intermolecular interactions. Detailed explanations for these interaction parameters are given in the subsequent section.

Eq. (7) is used to calculate for properties under the gas phase.

$$\mu_i^G = \mu_i^{G,0}(T) + RT \ln(P, y_i \varphi_i(T, P)/P^0) \quad (7)$$

Wherein  $\mu_i^{G,0}(T)$  is the chemical potential of pure component  $i$  under the ideal condition,  $y_i$  is gas state mole fraction,  $\varphi_i(T, P)$  is the fugacity coefficient defined in the enhanced, Soave-Redlich-Kwong (SRK) cubic equation of state (EoS) [21,29].  $P$  represents the total pressure; the reference state  $P^0$  is equivalent to 1 atm. In addition, OLI Analyzer computes all gas properties and its composition using the enhanced, SRK EoS. Define:

$$P = \frac{RT}{V-b} - \frac{a}{V(V+b)} \quad (8)$$

$R$  represents the ideal gas constant in L·atm/mol·K;  $T$  is the temperature in Kelvin,  $V$  is the total volume;  $a$  and  $b$  are set to 0 under the ideal gas condition, but a solution containing dissociated electrolyte would alter these parameters. The computations for  $a_{ij}$  are shown in Eqs. (9) and (10).

$$a = \sum_i \sum_j x_i x_j a_{ij} \quad (9)$$

$$a_{ij} = \sqrt{a_i a_j} (a - k_{ij}) \quad (10)$$

Specifically,  $k_{ij}$  can be correlated using Eq. (12).  $k_{ij0}$ ,  $k_{ij1}$ ,  $k_{ij2}$  are the interaction parameters used in the Kabadi-Danner extensions for the calculation of fugacity coefficients in SRK EoS.

$$H_2O(vap) = CO_2(vap) \quad (11)$$

$$k_{ij} = k_{ij0} + k_{ij1} * T + k_{ij2}/T \quad (12)$$

### 3.3. The activity coefficient model

An accurate model describing the solid-liquid system in the aqueous phase must consider the strong interaction contributed by the dissociated electrolytes. The Mixed-Solvent Electrolyte model (MSE) embedded in the OLI Analyzer provides an algorithm for the computation of interactions parameters resulting from the ion dissociation reactions [21]. A non-ideal solution is formed when a solute is added to the aqueous amine system; hence, the excess part denoted by  $G^E$  must be included in addition to the reference state, Gibbs Free Energy of an ideal mixture. A typical  $G^E$  expression is given in Eq. (13).

$$\frac{G^E}{RT} = \frac{G_{LR}^E}{RT} + \frac{G_{MR}^E}{RT} + \frac{G_{SR}^E}{RT} \quad (13)$$

The key feature of the MSE model is the inclusion of the 3 major components for the calculation of  $G^E$  [30]. Herein,  $G_{LR}^E$  stands for long-range electrostatic interactions, first derived and explained by the Debye-Hückel Theory.  $G_{SR}^E$  represents short-range interactions, drawn basis from the local composition model (UNIQUAC) for neutral interactions molecular interactions.  $G_{MR}^E$  considers the size:  $r$ , and the surface area:  $q$  of molecules to compute for the short-ranged, interactions.  $G_{MR}^E$  is the most important component as of solubility data parameterization, it accounts for all interactions not only between ion pairs, but also between molecule-ion and molecule pairs [21–22,30–31]. The general  $G_{MR}^E$  expression to correlate for a multi-component system is shown in Eq. (14).

$$\frac{G_{MR}^E}{RT} = - \left( \sum_i n_i \right) \sum_i \sum_j x_i x_j B_{ij}(I_x) \quad (14)$$

In addition, contribution of each individual ion is directly related to the ionic strength,  $I_x$  (in mol.-fraction), a larger ionic strength typically results in a smaller activity coefficient  $\gamma_i$ .  $B_{ij}(I_x)$  is a second-type virial, symmetrical parameter, i.e.:  $B_{ij}(I_x) = B_{ji}(I_x)$ ,  $B_{ii} = B_{jj} = 0$ , this further indicates that the sequence of entering raw data does not affect the parameter values.

$$B_{ij}(I_x) = [b_{ij,1} + b_{ij,2}(T - T_0)] + [c_{ij,1} + c_{ij,2}(T - T_0)] \exp(-\sqrt{I_x + 0.01}) \quad (15)$$

Data regressions were done by utilizing the objective functions shown in Eqs. (16) and (17). The regression method selected is Brown's algorithm, (Marquardt scaling parm: METH = 0).  $b_{ij}$  and  $c_{ij}$  are binary interaction parameters, both are expressed as a function of temperature.

$$b_{ij} = b_{0,ij} + b_{1,ij}T + \frac{b_{2,ij}}{T} \quad (16)$$

$$c_{ij} = c_{0,ij} + c_{1,ij}T + \frac{c_{2,ij}}{T} \quad (17)$$

Lastly, the activity coefficient of ion  $\gamma_i$  must be considered to account for the deviation from an ideal mixture. Thermodynamic relation between the activity coefficient of ion and  $G^E$  is related by the differential equation as stated in Eq. (18).

$$\ln \gamma_i = \left[ \frac{\partial n G^E / RT}{\partial n_i} \right]_{P, T, n_j} \quad (18)$$

### 3.4. Solubility product constant: $K_{SP}$

One major objective of this work is to investigate the solubility of salts: K<sub>2</sub>CO<sub>3</sub> and KHCO<sub>3</sub>, solely dissolve in the aqueous MEA or DEA solution. Specifically, for each salt equilibrated dissociation, the solubility product constant [30], aka.  $K_{sp}$  is generally quantified as a temperature-dependent only constant. For this value, it can be derived either from the Van't Hoff Equation, which is directly related to the standard-state properties, or computed through the MSE, activity coefficient model. The calculation for the later method is shown in Eq. (19).

$$K_{SP} = \prod a_i^{\nu_i} = \prod \gamma_{\pm}^{\nu_i} m_i^{\nu_i} a_{H_2O} \quad (19)$$

Eqs. (20) and (21) are the corresponding  $K_{sp}$  calculations for K<sub>2</sub>CO<sub>3</sub> and KHCO<sub>3</sub>.  $K_{sp}$  values are directly related to the activity coefficient of each ion.

$$K_{SP, K_2CO_3} = a_{K^+}^2 a_{CO_3^{2-}} = (m_{K^+}^2 \gamma_{K^+}^2) \cdot (m_{CO_3^{2-}} \gamma_{CO_3^{2-}}) \quad (20)$$

$$K_{SP, KHCO_3} = a_{K^+} a_{HCO_3^-} = (m_{K^+} \gamma_{K^+}) \cdot (m_{HCO_3^-} \gamma_{HCO_3^-}) \quad (21)$$

The empirical equation of calculating  $K_{sp}$  is presented in Eq. (22). Under which parameters  $A$ ,  $B$ ,  $C$  and  $D$  were experimentally determined. Parameters  $A$ – $D$  for both solutes [21], along with a list of

**Table 3**  
Standard-State Thermodynamic Properties (OLI MSE Model).

Species	$\Delta G_{f,298}^0$ (cal/mol)	$\Delta H_{f,298}^0$ (cal/mol)	$\Delta S_{298}^0$ (cal/mol/C)	$\Delta C_{P,298}^0$ (cal/mol/C)
H <sub>2</sub> O	-56689	-68315	16.72	18.00
K <sup>+</sup>	-67510	-60270	24.15	1.98
CO <sub>3</sub> <sup>2-</sup>	-126191	-161385	-11.95	-69.50
HCO <sub>3</sub> <sup>-</sup>	-140282	-164898	23.53	-8.46
KOH (aq)	-87761	-82304	73.86	-20.50
OH <sup>-</sup>	-37595	-54968	-2.56	-32.79
H <sup>+</sup>	-56686	-68305	16.73	18.00
C <sub>4</sub> H <sub>11</sub> NO <sub>2</sub> (aq)	-63010	-119624	59.13	78.08
C <sub>4</sub> H <sub>12</sub> NO <sub>2</sub> <sup>+</sup>	-75142	-129442	66.89	57.83
C <sub>5</sub> H <sub>10</sub> NO <sub>4</sub> <sup>-</sup>	-147579	-222138	49.32	136.18
C <sub>2</sub> H <sub>7</sub> NO (aq)	-32626	-67595	42.07	44.22
C <sub>2</sub> H <sub>8</sub> NO <sup>+</sup>	-44833	-78974	44.82	44.22
C <sub>3</sub> H <sub>6</sub> NO <sub>3</sub> <sup>-</sup>	-118406	-164380	55.92	69.54
CO <sub>2</sub> (aq)	-92250	-98900	28.10	58.10
CO <sub>2</sub> (g)	-94254	-94051	51.09	8.88
<i>K<sub>sp</sub></i> (T)	A	B	C	D
K <sub>2</sub> CO <sub>3</sub> (s)	-1.14919	2904.32	0.00571	-2.8E-5
KHCO <sub>3</sub> (s)	-1.5925	-814.706	0.009536	-1.6E-5

\*MEA is equivalent to C<sub>2</sub>H<sub>7</sub>NO; DEA is equivalent to C<sub>4</sub>H<sub>11</sub>NO<sub>2</sub> [21].

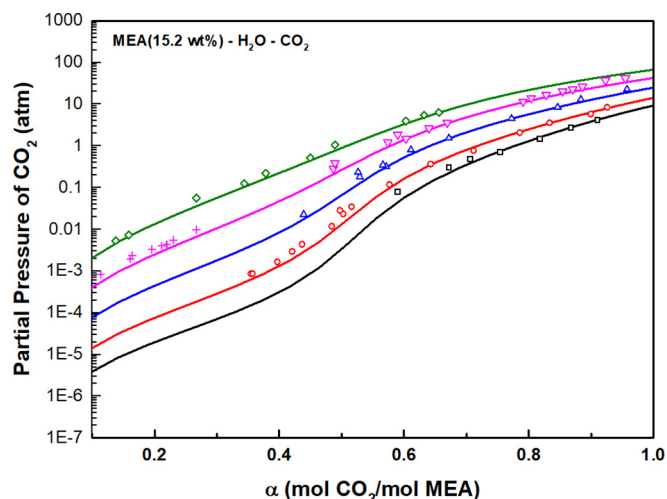
thermodynamic properties for each species are listed in Table 3.

$$\log(K_{sp}) = A + \frac{B}{T} + CT + DT^2 \quad (22)$$

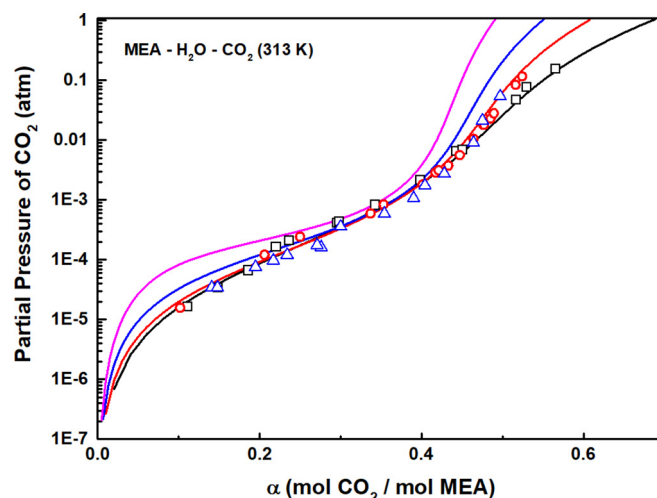
## 4. Results/discussion

### 4.1. Model validation – VLE calculation

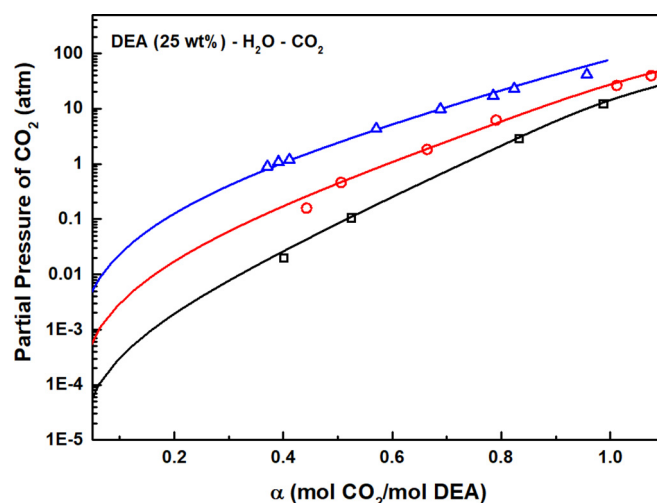
The VLE data used in model validation are for ternary systems containing amine, water and CO<sub>2</sub>, graphically represented as the  $P_{CO_2}$  as a function of CO<sub>2</sub> loading/amine. Figs. 2–6 present the modeling results for the calculated  $P_{CO_2}$  for the following systems: MEA-H<sub>2</sub>O-CO<sub>2</sub> [32–37], and DEA-H<sub>2</sub>O-CO<sub>2</sub> [38] and K<sub>2</sub>CO<sub>3</sub>-H<sub>2</sub>O-CO<sub>2</sub> [14,35]. These data are not measured in this work, but are correlated based on the initialized, default parameters from the existing MSE model databank; calculated results are further plotted against literature data. First, the vapor-liquid equilibrium for the systems MEA-H<sub>2</sub>O-CO<sub>2</sub> are shown in Figs. 2 and 3. The match in precision of the model and data points from



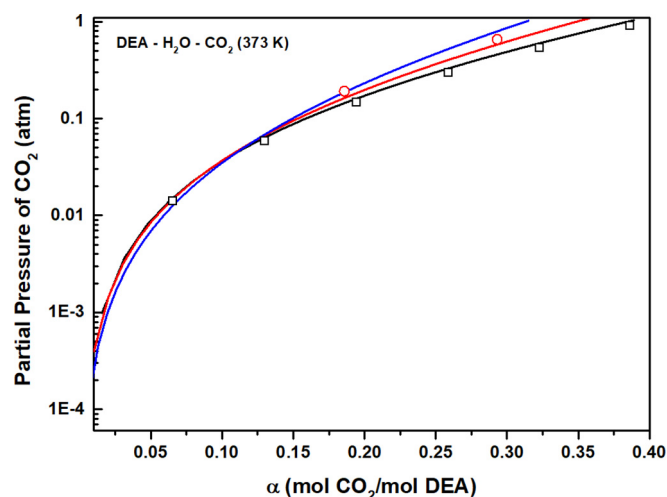
**Fig. 2.** MSE model calculation for the solubility of CO<sub>2</sub> in 15.2 wt% aqueous MEA solution at (■) 298 K; (●) 313 K; (▲) 333 K; (◆) 353 K; (◆) 373 K; with comparison to the reported literature data: (□) Lee et al.; (○) Austgen et al.; (△) Jones et al.; (▽) Bhairi et al.; (+) Nathier & Mather et al.; (◇) Jones et al.



**Fig. 3.** MSE model calculation for the solubility of CO<sub>2</sub> in the aqueous MEA solution at (■) 15 wt%; (●) 30 wt%; (▲) 45 wt%; (◆) 60 wt% when  $T = 313$  K; with comparison to the reported literature data from Aronu et al.



**Fig. 4.** MSE model calculation for the solubility of CO<sub>2</sub> in 25 wt% aqueous DEA solution at (■) 298 K; (●) 313 K; (▲) 333 K; with comparison to the reported literature data (open symbols) from Lawson & Garst.



**Fig. 5.** MSE model calculation for the solubility of CO<sub>2</sub> in the aqueous DEA solution at (■) 16.7 wt%; (●) 25.9 wt%; (▲) 35 wt% when  $T = 373$  K; with comparison to the reported literature data (open symbols) from Bhairi et al.



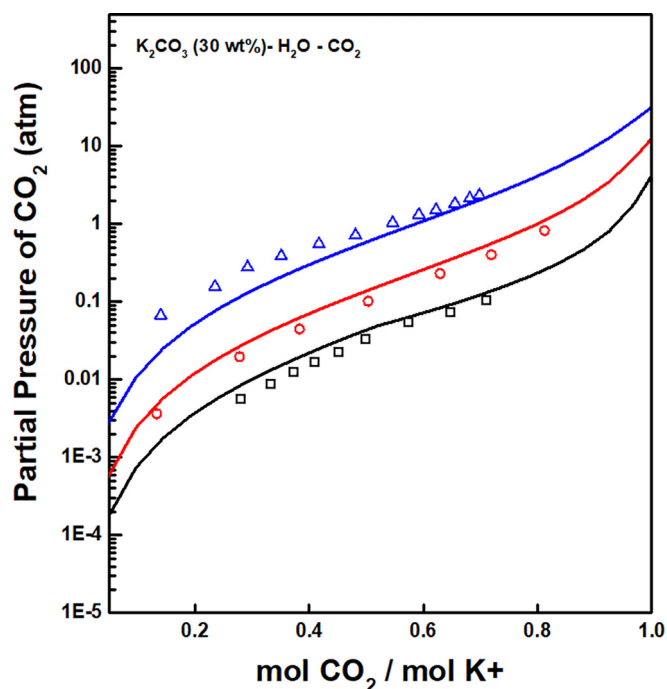


Fig. 6. MSE model calculation for the solubility of  $\text{CO}_2$  in 30 wt% aqueous  $\text{K}_2\text{CO}_3\text{-H}_2\text{O}$  solution at (■) 313 K; (●) 343 K; (▲) 393 K with comparison to the reported experimental data (open symbols) by Gao et al.

literature works are fair, for which these partial pressures are for low to high  $\text{CO}_2$  loading, and a low to high in temperature range (298–373 K). In general,  $P_{\text{CO}_2}$  shows a strong relationship dependent upon both

temperature and the concentration of amine solution. If temperature is raised from 298 K to 373 K. The pressure needed to keep  $\text{CO}_2$  dissolved moves up substantially (plotted in log. scale). As shown in Fig. 3,  $P_{\text{CO}_2}$  tends to drop with an increase in MEA concentration when the simulated temperature (313 K) stays constant. The calculated  $P_{\text{CO}_2}$  shows good consistency for 15 wt% and 30 wt% compared to literature data. The model slightly overpredicts  $P_{\text{CO}_2}$  at a higher loading region using 45 wt% MEA, but gives no error determining where the point of inflection appears, a condition when the slope of the absorption profile increases exponentially.

As shown in Fig. 4, we observed a similar absorption profile for the system DEA (25 wt%)- $\text{H}_2\text{O}\text{-CO}_2$  compared to that of MEA. However, Fig. 5 gives an example such that a cross-over of the curve was observed at  $\alpha = 0.125$  at  $T = 353$  K, this leads to the fact that adding more DEA into the solution increases the solubility of  $\text{CO}_2$  into the bulk liquid by forming carbamate. Literature values are graphically represented in these figures as well, further confirmed the consistency of the MSE model capable of reproducing the absorption behavior of  $\text{CO}_2$  in the DEA solution.

Lastly, the promotion of using carbonate solution, aka. “the hot potash” solution, without the use of amines were also proven to be particularly effective for a typical gas scrubbing process in terms of loading capacity. Fig. 6 illustrates the simulated results for the absorption profile of  $\text{CO}_2$  under a 30 wt% of  $\text{K}_2\text{CO}_3$  loading. At the same  $P_{\text{CO}_2}$ , the loading of  $\text{CO}_2$  shifts leftward, this indicates that  $\text{CO}_2$  loading decreases if temperature is raised from 313 K to 393 K; a high temperature is only favorable for a typical desorption process to occur. Other factors, such as surface tension, heat capacity and viscosity may also influence the rate of absorption as well as the loading capacity of  $\text{CO}_2$ .

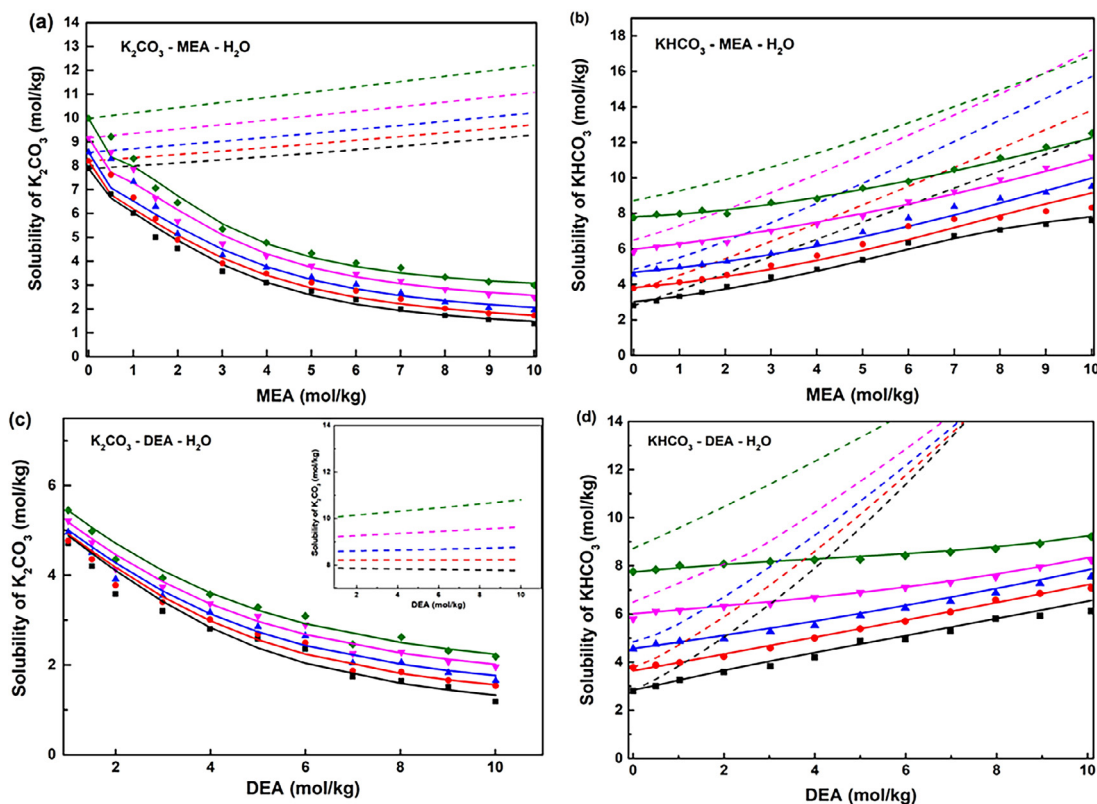


Fig. 7. (a) The solubility of  $\text{K}_2\text{CO}_3$  in the aqueous MEA solution; (b) the solubility of  $\text{KHCO}_3$  in the aqueous MEA solution; (c) the solubility of  $\text{K}_2\text{CO}_3$  in the aqueous DEA solution; (d) the solubility of  $\text{KHCO}_3$  in the aqueous DEA solution at (■) 283 K, (●) 298 K, (▲) 313 K, (▼) 333 K, (◆) 353 K;  $P = 0.1$  MPa; dashed lines: old model calculation; dots: experimental data; solid lines: new model calculation.

#### 4.2. Solubility measurements for SLE systems: $K_2CO_3$ -MEA- $H_2O$ , $KHCO_3$ -MEA- $H_2O$ , $K_2CO_3$ -DEA- $H_2O$ , $KHCO_3$ -DEA- $H_2O$

The solubility of inorganic salts in the aqueous MEA and DEA solution had been successfully measured for many systems [39,40]; possible relevance to the carbonate system:  $K$ - $HCO_3$ - $CO_3$  in alkanolamines solutions is yet to be investigated. Particular thermodynamic behavior, and the need to determine the maximum potential loading of potassium salt in alkanolamine solutions encouraged the present study to test out their solubility in four, solid-liquid systems:  $K_2CO_3$ -MEA- $H_2O$ ,  $KHCO_3$ -MEA- $H_2O$ ,  $K_2CO_3$ -DEA- $H_2O$ ,  $KHCO_3$ -DEA- $H_2O$ . Data tables are subsequently displayed in Tables S1–S4, and graphically represented in Fig. 7(a)–(d).

Solubility measurements were taken from 298 to 353 K under the amine concentration of 0–10 mol/kg. In general, adding more amine into the solution reduces the solubility of  $K_2CO_3$ , hereafter  $K_2CO_3$  precipitates in the form of hydrate [12]. In contrary, the SLE correlation for the ternary system containing  $KHCO_3$  shows a different pattern, for which an increased concentration of amine makes  $KHCO_3$  more soluble. For both systems, solubility and temperature are positively related. Experimental data are presented in Tables S1–S4. It is important to note that  $KHCO_3$  often precipitate at intermediate temperature, knowing the maximum solubility of  $KHCO_3$  would avoid typical clogging problem at the bottom of the absorber. Within the context of limitation, future investigations may fulfill and to expand the dataset if conducting similar experiments at higher temperature or pressure.

For all cases, the initial solubility predicted by OLI were inaccurate as indicated by the dashed line drawn for each system, but results are far much better after reparameterization. The pair-wise, binary middle-range interactions adjusted for thermodynamic modeling are:  $K^+$ -MEA,  $K^+$ - $MEACOO^-$ ,  $HCO_3^-$ -DEA,  $K^+$ -DEA,  $K^+$ - $DEACOO^-$ , other interaction parameters stay as default in the MSE databank [21–22,40]. These newly-adjusted parameters were incorporated to re-correlate the SLE data for these systems. A list of parameters is shown in Table 4. We performed statistical analysis to quantitatively measure the differences between experimental data and the regressed results, details are

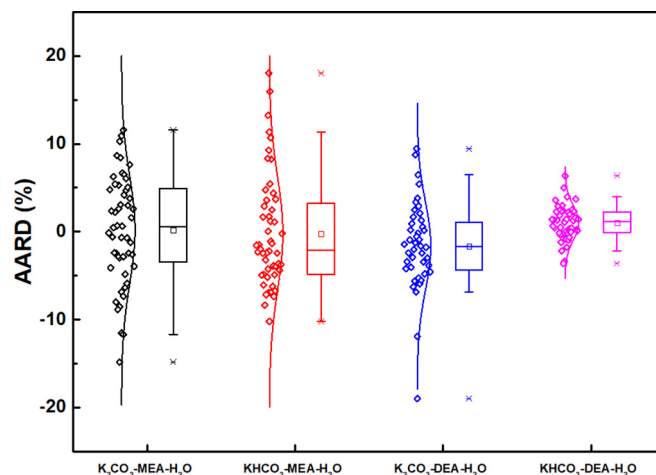


Fig. 8. The absolute, averaged relative deviation (AARD%) of the solid-liquid equilibrium systems.

unveiled in the subsequent section.

#### 4.3. Statistical analysis: solid-liquid system

The interaction parameters after data regression were determined for each of the ternary, solid-liquid system. As shown in Fig. 8, relative standard deviations for each system are graphically represented in the form of box plots. Whiskers were drawn to extend the differences of values between the 25th percentile (lower) – 75th percentile (upper). The 50th percentile is indicated by a line as shown within the whisker box.  $n$  represents the total number of experimental data. The calculation method [41] for the overall averaged, absolute, relevant deviation (AARD):  $\sigma$  between experimental data  $X_{i,exp}$  and the calculated value  $X_{i,calc}$  is shown in Eq. (23).

Table 4  
The Binary Interaction Parameters (MSE Model).

Virial Interaction Parameters (Middle-Range)							
Species <sup>a</sup>		BMD0	BMD1	BMD2	CMD0	CMD1	CMD2
$HCO_3^-$	$K^+$	−64.26117	0.09827565	10603.65	0.224879	0.0046471	1665.383
$CO_3^{2-}$	$K^+$	103.865	−0.127249	−29244.1	−322.264	0.46417	71799.4
MEA	$K^+$	−29.68244	−0.06022356	−12147.16	49.84969	0.2168208	−502.8127
$MEACOO^-$	$K^+$	40.2151	0.4911801	−200891.6	847.8267	−3.037119	60,413
$MEACOO^-$	$HCO_3^-$	5577.035	−8.619752	−901912.8	−8056.631	12.45682	1,304,147
MEA $H^+$	$HCO_3^-$	190.2563	−0.662543	519.8183	−282.3155	0.996023	0
MEA $H^+$	$MEACOO^-$	−144.0274	0.411181	0	211.5554	−0.633781	0
DEA	$K^+$	−22.21572	0.1592838	−15153.47	170.484	−0.4304486	−5684.53
$DEACOO^-$	$K^+$	0	−0.1966877	0	0	0	0
DEA	$HCO_3^-$	881.3923	−1.416084	−182008.8	154.7746	0.05789678	4202.984
$DEACOO^-$	$HCO_3^-$	−12.71294	0.0	5907.997	0	0	0
DEA $H^+$	$HCO_3^-$	−71.44205	0.08492444	7241.57	36.38963	0	0
DEA	$DEACOO^-$	0.634883	0	−979.6115	0	0	0
UNIQUAC Parameters (Short-Range)							
Species		$Q0_{IJ}$	$Q0_{JI}$	$Q1_{IJ}$	$Q1_{JI}$	$Q2_{IJ}$	$Q2_{JI}$
DEA	$H_2O$	−874.2494	−2178.758	12.28852	0.524225	0.0020072	−0.005172
MEA	$H_2O$	819.6007	−2336.405	0.274377	4.655944	0	0
$CO_2$	$H_2O$	−3439.31	7331.98	0.032772	−29.5063	0	0
SRK parameters							
Species		$k_{ij0}$	$k_{ij1}$	$k_{ij2}$	$g_{ij}$		
$CO_2$	$H_2O$	0.3750704	0	−8.836687	0		

<sup>a</sup> Species pairs  $K^+$ -MEA,  $K^+$ - $MEACOO^-$ ,  $HCO_3^-$ -DEA,  $K^+$ -DEA,  $K^+$ - $DEACOO^-$  were reparameterized; others are kept as default parameters in OLI ESP.

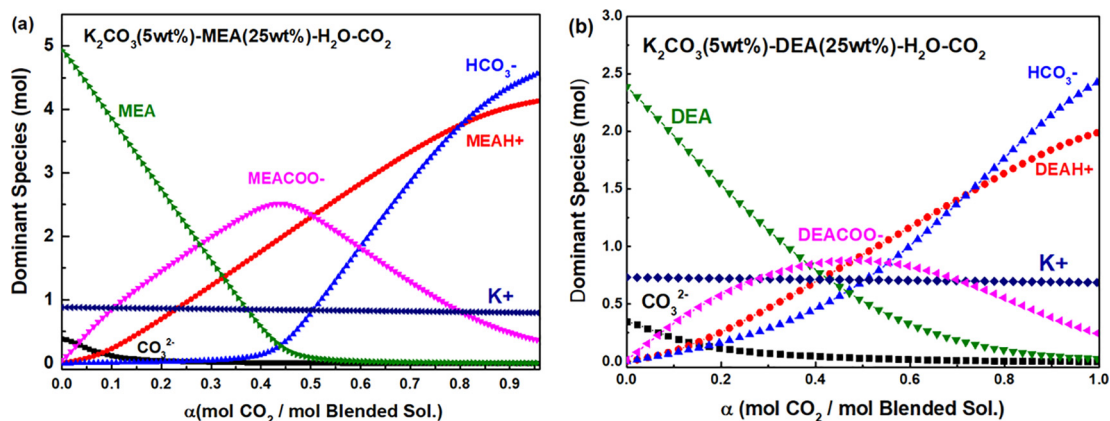


Fig. 9. Speciation of dominant ions for the system (a)  $K_2CO_3$ -MEA- $H_2O$ - $CO_2$  at  $T = 313$  K,  $P = 0.1$  Mpa (b)  $K_2CO_3$ -DEA- $H_2O$ - $CO_2$  at  $T = 313$  K,  $P = 0.1$  Mpa.

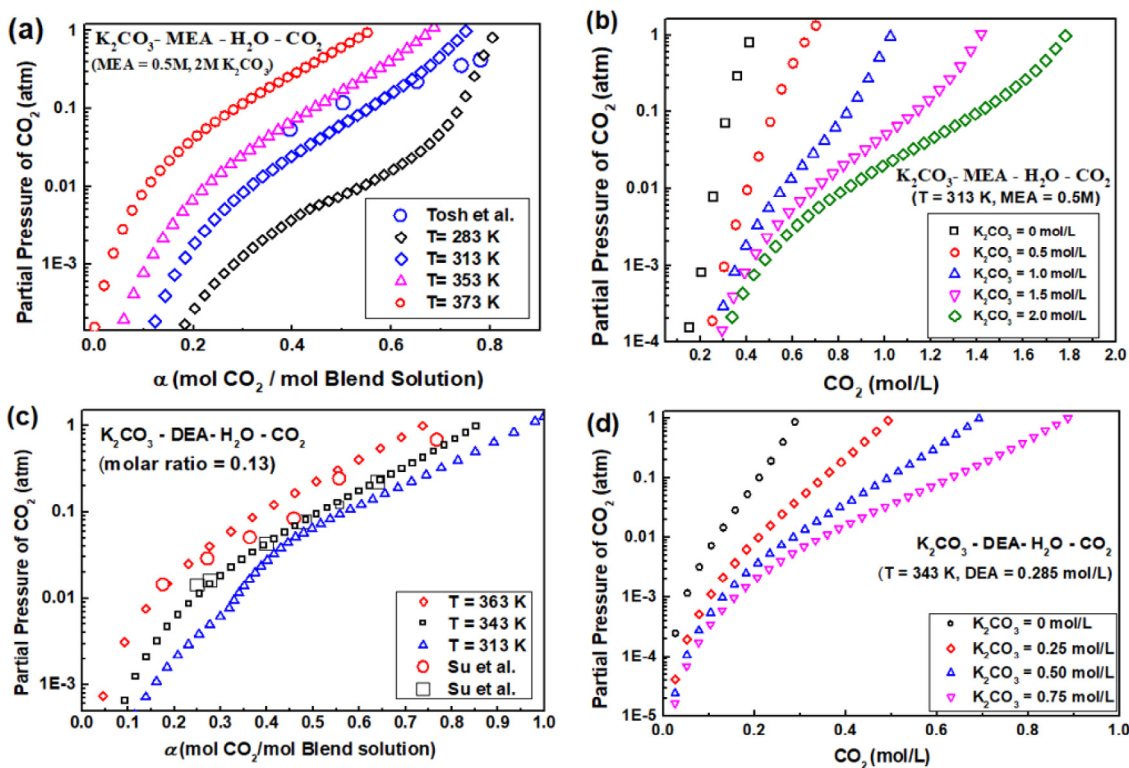


Fig. 10. (a)  $P_{CO_2}$  vs.  $\alpha$  at molar ratio = 0.25; (b)  $P_{CO_2}$  vs.  $\alpha$  at different concentration of  $K_2CO_3$ . (c)  $P_{CO_2}$  vs.  $\alpha$  at molar ratio = 0.13; (d)  $P_{CO_2}$  vs.  $\alpha$  at different concentration of  $K_2CO_3$ .

$$\bar{\sigma} = 100/n \sum_{i=1}^n \left| \frac{X_{i,calc} - X_{i,exp}}{X_{i,exp}} \right| \quad (23)$$

The  $\bar{\sigma}$  calculated for the system:  $K_2CO_3$ -MEA- $H_2O$ ,  $KHCO_3$ -MEA- $H_2O$ ,  $K_2CO_3$ -DEA- $H_2O$ ,  $KHCO_3$ -DEA- $H_2O$  are 5.00%, 5.14%, 3.90% and 1.65%, respectively. For all systems, the standard uncertainty for temperature, solubility, and temperature are  $u(T) = 0.15$  K,  $u(m) = 0.2$  mol·kg<sup>-1</sup>,  $u(P) = 0.5$  kPa, respectively.

#### 4.4. Speciation modeling of quaternary systems

Speciation modeling of an equilibrated system can be highly informative, in conjunction with the MSE model does it allow a vivid description of ion complexation and the change in concentration. Since most reported studies tend to focus on the speciation analysis only for a typical amine- $CO_2$  system, this model is advantageous for a clear visualization of the speciation distribution regarding the quaternary

systems:  $K_2CO_3$ -amine- $H_2O$ - $CO_2$ . The modeling condition is fixed at 313 K, with a 25 wt% amine and a 5 wt%  $K_2CO_3$ . Results are presented in Fig. 9(a) & (b).

First, we discerned an immediate reduction in the amine concentration as the solution is loaded with more  $CO_2$  [24,37]. At a lower loading, practically for  $\alpha < 0.45$ , all  $CO_2$  bind with carbamate and the formed carbamate during the absorption process increases almost linearly until  $\alpha$  approaches 0.45. During the absorption process, the protonated species:  $MEA^+$  or  $DEAH^+$  increases at the expense of consuming the unprotonated amines themselves. Bypassing a loading of 0.45 we still witnessed a continued rise in the protonated species, but the true concentration of carbamate species plummeted. The  $CO_2$  being released from the carbamates began to react with  $HCO_3^-$ . In the presence of  $K_2CO_3$ , the bicarbonate ion concentration in solvents increases with higher  $CO_2$  loadings, this explains an increase in solubility for  $KHCO_3$ .

In contrast, a rise in the  $HCO_3^-$  concentration for the DEA system



begins at a  $\alpha$  value ahead of the MEA system. Also, the concentration of all species in the DEA system are systematically lower at the same temperature and  $\alpha$ . This observation stems from the fact that the molecular weight of DEA is much higher than that of MEA, thus resulting in more available amine group and thus forming less carbamate. The concentration of  $K^+$  stays constant for both systems, this indicate that there is no additional ion complex formed by the addition of potassium.

#### 4.5. Model application: absorption performance of $CO_2$ in amine-promoted solutions

One of the most important tasks of this study is to apply the constructed model into forecasting the absorption performance of  $CO_2$  in amine-promoted, potassium carbonate solution. The effect of  $CO_2$  loading, temperature, and the composition of amine can be studied for the quaternary system based on the newly-constructed model.

First, graphical representations for the solubility of  $CO_2$  into MEA-promoted, carbonate solution are shown in Fig. 10(a) & (b). At a molar ratio of 0.25, which is equivalent to 0.5 mol. of MEA and 2 mol. of  $K_2CO_3$ , the calculated results at 313 K are compared to a study reported by Tosh et, al [42,43]. The  $P_{CO_2}$  was plotted in log. scale so a seemingly small deviation may appear large graphically. Results highlight the fact that an increase in temperature results in a decrease in  $CO_2$  loading at the same  $P_{CO_2}$ . At a constant temperature, we clearly visualized that the loading capacity enhances if  $P_{CO_2}$  is being increased. What the figure does not show is the Henry's constant and surface tension. Due to the corresponding  $CO_2$  diffusivity for a solution containing  $K_2CO_3$  and amine are less than those for a single amine, and thus DEA outperforms a promoted  $K_2CO_3$  solution in terms of reaction rate. As shown in Fig. 10(c) & (d), the DEA-promoted, carbonate solution was plotted similarly for comparison purposes [44].

## 5. Conclusions

In evaluating the absorption performance of  $CO_2$  in quaternary systems that includes the hot, potassium carbonate solution promoted with MEA or DEA, this work provides detailed, thermodynamic analysis to aid in the modeling effort. Through the VLE calculation for the partial pressure of  $CO_2$  vs. the loading capacity:  $\alpha$  (mol  $CO_2$ /mol amine), we first confirmed that the existing VLE parameters for the systems: MEA- $H_2O$ - $CO_2$  and DEA- $H_2O$ - $CO_2$  were accurate. Solubility experiments for the solid-liquid systems regarding  $K_2CO_3$  and  $KHCO_3$  in the aqueous MEA, DEA solution from 283 to 353 K,  $P = 0.1$  MPa were conducted. One, thus, is led to the following conclusion: an increase in temperature would enhance the solubility of both solutes, whereas an increase in amine concentration tends to lower the solubility of  $K_2CO_3$ , yet makes  $KHCO_3$  more soluble when temperature is held constant. The relative deviations between the experimental and the calculated data are within 5% for each SLE system after the interaction parameters were optimized. The speciation distribution profiles for the quaternary systems were provided, which aid in the effort to visualize the formation of carbamate, as well as the dissociation behaviors for other ions due to chemical reactions.

## Acknowledgements

The authors are grateful for the financial support provided by the National Science Foundation of China (Grants 21776279 and 21978290). The authors declare no competing financial interest.

## Declaration of interests

None

## Appendix A. Supplementary data

Supplementary data to this article can be found online at <https://doi.org/10.1016/j.cej.2019.123250>.

## References

- [1] P.L. Mores, J.I. Manassaldi, N.J. Scenna, J.A. Caballero, M.C. Mussati, S.F. Mussati, Optimization of the design, operating conditions, and coupling configuration of combined cycle power plants and  $CO_2$  capture processes by minimizing the mitigation cost, *Chem. Eng. J.* 331 (2018) 870–894.
- [2] C. Lastoskie, Caging carbon dioxide, *Science* 330 (2010) 595–596.
- [3] H. Waisman, C. Bataille, H. Winkler, et al., A pathway design framework for national low greenhouse gas emission development strategies, *Nature Climate Change* 9 (2019) 261–268.
- [4] S. Nandi, P. De Luna, T.D. Daff, J. Rother, M. Liu, W. Buchanan, A.I. Hawari, T.K. Woo, R. Vaidhyanathan, A single-ligand ultra-microporous MOF for pre-combustion  $CO_2$  capture and hydrogen purification, *Sci. Adv.* 1 (2015) e1500421.
- [5] T.E. Akinola, E. Oko, M. Wang, Study of  $CO_2$  removal in natural gas process using mixture of ionic liquid and MEA through process simulation, *Fuel* 236 (2019) 135–146.
- [6] G. Lin, S. Jiang, C. Zhu, T. Fu, Y. Ma, Mass-transfer characteristics of  $CO_2$  absorption into aqueous solutions of N-methyldiethanolamine + diethanolamine in a T-junction microchannel, *ACS Sustainable Chem. Eng.* 7 (2019) 4368–4375.
- [7] M. Xiao, W. Zheng, H. Liu, P. Tontiwachwuthikul, Z. Liang, Analysis of equilibrium  $CO_2$  solubility and thermodynamic models for aqueous 1-(2-hydroxyethyl)-piperidine solution, *AIChE J.* 65 (2019) e16605.
- [8] I.I.I. Alkhatib, L.M.C. Pereira, L.F. Vega, 110th anniversary: accurate modeling of the simultaneous absorption of  $H_2S$  and  $CO_2$  in aqueous amine solvents, *Ind. Eng. Chem. Res.* 58 (2019) 6870–6886.
- [9] T.B.H. Nguyen, E. Zondervan, Ionic liquid as a selective capture method of  $CO_2$  from different sources: comparison with MEA, *ACS Sustainable Chem. Eng.* 6 (2018) 4845–4853.
- [10] B. Xue, Y. Yu, J. Chen, X. Luo, M. Wang, A comparative study of MEA and DEA for post-combustion  $CO_2$  capture with different process configurations, *Int. J. Coal Sci. Technol.* 4 (2017) 15–24.
- [11] G. Astarita, D.W. Savage, J.M. Longo, Promotion of  $CO_2$  mass transfer in carbonate solutions, *Chem. Eng. Sci.* 36 (1981) 581–588.
- [12] P.L. Fosbol, B. Maribo-Mogensen, K. Thomsen, Solids modelling and capture simulation of piperazine in potassium solvents, *Energy Procedia* 37 (2013) 844–859.
- [13] L. Petrescu, D. Bonalumi, G. Valenti, A.M. Cormos, C.C. Cormos, Life Cycle Assessment for supercritical pulverized coal power plants with post-combustion carbon capture and storage, *J. Clean. Prod.* 157 (2017) 10–21.
- [14] S. Gao, D. Guo, H. Jin, S. Li, J. Wang, S. Wang, Potassium carbonate slurry-based  $CO_2$  capture technology, *Energy Fuels* 29 (2015) 6656–6663.
- [15] S.S. Laddha, P.V. Dancwerts, The absorption of  $CO_2$  by amine-potash solutions, *Chem. Eng. Sci.* 37 (1982) 665–667.
- [16] A.S. Berrouk, B. Ochieng, Improved performance of the natural-gas-sweetening Benfield-HiPure process using process simulation, *Fuel Process. Technol.* 127 (2014) 20–25.
- [17] H.E. Benson, R.W. Parrish, HiPure process removes  $CO_2/H_2S$ , *Hydrocarbon Process.* 53 (1974) 81–82.
- [18] P. Wang, J.J. Kosinski, A. Anderko, R.D. Springer, M.M. Lencka, J. Liu, Ethylene glycol and its mixtures with water and electrolytes: thermodynamic and transport properties, *Ind. Eng. Chem. Res.* 52 (2013) 15968–15987.
- [19] Y. Zeng, Z. Li, Solubility measurement and modeling for the  $NaCl-NH_4Cl$ -monoethylene glycol- $H_2O$  system from (278 to 353) K, *J. Chem. Eng. Data* 60 (2015) 2248–2255.
- [20] J. Zhou, Y. Zeng, G.P. Demopoulos, C. Li, Z. Li, Phase Transition of  $FeSO_4 \cdot 7H_2O$  to  $FeSO_4 \cdot H_2O$  in the  $H_2SO_4$ -HCl- $H_2O$  system by modeling solubility, *ACS Sustainable Chem. Eng.* 6 (2018) 2207–2219.
- [21] OLI Systems, Inc., OLI Analyzer Studio – Stream Analyzer version 9.5, <http://www.olisystems.com>. Accessed June 17, 2019.
- [22] OLI System Inc. OLI ESP user guide – A guide to using OLI ESP 9.X, <http://support.olisystems.com>. Accessed June 17, 2019.
- [23] H. Thee, Y.A. Suryaputradinata, K.A. Mumford, K.H. Smith, G. da Silva, S.E. Kentish, G.W. Stevens, A kinetic and process modeling study of  $CO_2$  capture with MEA-promoted potassium carbonate solutions, *Chem. Eng. J.* 210 (2012) 271–279.
- [24] Y. Liu, L. Zhang, S. Watanasiri, Representing vapor–liquid equilibrium for an aqueous MEA- $CO_2$  system using the electrolyte nonrandom-two-liquid model, *Ind. Eng. Chem. Res.* 38 (1999) 2080–2090.
- [25] Y. Zhang, H. Chen, C.-C. Chen, J.M. Plaza, R. Dugas, G.T. Rochelle, Rate-based process modeling study of  $CO_2$  capture with aqueous monoethanolamine solution, *Ind. Eng. Chem. Res.* 48 (2009) 9233–9246.
- [26] Z. Cai, R. Xie, Z. Wu, Binary isobaric vapor–liquid equilibria of ethanolamines + Water, *J. Chem. Eng. Data* 41 (1996) 1101–1103.
- [27] H.C. Helgeson, D.H. Kirkham, G.C. Flowers, Theoretical Prediction of the Thermodynamic Behavior of Aqueous Electrolytes at High Pressures and Temperatures, *Kline Geology Laboratory, Yale University*, 1981.
- [28] J.C. Tanger, H.C. Helgeson, Calculation of thermodynamic and transport properties of aqueous species at high pressures and temperatures: revised equations of state for the standard partial molal properties of ions and electrolytes, *Am. J. Sci.* 288 (1988) 19–98.

- [29] G. Soave, Equilibrium constants from a modified Redlich-Kwong equation of state, *Chem. Eng. Sci.* 27 (1972) 1197–1203.
- [30] J.F. Zemaitis, D.M. Clark, M. Rafal, N.C. Scrivner, *Handbook of Aqueous Electrolyte Thermodynamics*, first ed., AIChE Inc., New York, 1986.
- [31] D.S. Abrams, J.M. Prausnitz, Statistical thermodynamics of liquid mixtures: a new expression for the excess Gibbs energy of partly or completely miscible systems, *AIChE J.* 21 (1975) 116–128.
- [32] J.I. Lee, F.D. Otto, A.E. Mather, The solubility of  $H_2S$  and  $CO_2$  in aqueous monoethanolamine solutions, *Can. J. Chem. Eng.* 52 (1974) 803–805.
- [33] D.M. Austgen, G.T. Rochelle, X. Peng, C.C. Chen, Model of vapor-liquid equilibria for aqueous acid gas-alkanolamine systems using the electrolyte-NRTL equation, *Ind. Eng. Chem. Res.* 28 (1989) 1060–1073.
- [34] J.H. Jones, H.R. Froning, E.E. Claytor, Solubility of acidic gases in aqueous monoethanolamine, *J. Chem. Eng. Data* 4 (1959) 85–92.
- [35] A. Bhairi, Experimental equilibrium between acid gases and ethanolamine solutions. Ph.D. Thesis, Ohio State University, December 2004.
- [36] P. Nasir, A.E. Mather, The measurement and prediction of the solubility of acid gases in monoethanolamine solutions at low partial pressures, *Can. J. Chem. Eng.* 55 (1977) 715–717.
- [37] U.E. Aronu, S. Gondal, E.T. Hessen, T. Haug-Warberg, A. Hartono, K.A. Hoff, H.F. Svendsen, Solubility of  $CO_2$  in 15, 30, 45 and 60 mass% MEA from 40 to 120 °C and model representation using the extended UNIQUAC framework, *Chem. Eng. Sci.* 66 (2011) 6393–6406.
- [38] J.D. Lawson, A.W. Garst, Gas sweetening data: equilibrium solubility of hydrogen sulfide and carbon dioxide in aqueous monoethanolamine and aqueous diethanolamine solutions, *J. Chem. Eng. Data* 21 (1976) 20–30.
- [39] Q. Wang, Z. Li, Solubility determination and thermodynamic modeling for the system  $NaCl-NH_4Cl$ -diethanolamine- $H_2O$ , *J. Chem. Eng. Data* 64 (2019) 895–904.
- [40] H.L. Silcock, *Solubilities of Inorganic and Organic Compounds*, first ed., Pergamon Press, Oxford, 1979.
- [41] G.E.P. Box, W.G. Hunter, J.S. Hunter, *Statistics for Experimenters: An Introduction to Design, Data Analysis, and Model Building*, John Wiley & Sons, New York, 2005.
- [42] J.S. Tosh, J.H. Field, H.E. Benson, W.P. Haynes, *Equilibrium Study of the System Potassium Carbonate, Potassium Bicarbonate, Carbon dioxide, and Water*, BM-R1-5484, United States Bureau of Mines, Pittsburgh, PA, USA, 1959.
- [43] R. Ramazani, S. Mazinani, A. Jahanmiri, B. Van der Bruggen, Experimental investigation of the effect of addition of different activators to aqueous solution of potassium carbonate: absorption rate and solubility, *IJGGC* 45 (2016) 27–33.
- [44] Y. Su, X. Sun, X. Xu, W. Sun, A study on vapor-liquid equilibrium of amine – promoted carbonate solutions- $K_2CO_3-CO_2-H_2O-DEA$  system, *J. East China Univ. Sci. Technol.* 13 (1987) 27–37.